A Stretch-Coil Transition and Transport of Fibers in Cellular Flows

Y.-N. Young[1] and Michael Shelley[2]
[1] *Department of Mathematical Sciences, NJIT, Newark, NJ, 07102, USA*
[2] *Courant Institute of Mathematical Sciences, NYU, New York, NY, 10012, USA*
(Dated: April 12, 2007)

It is shown that a slender elastic fiber moving in a Stokesian fluid can be susceptible to a buckling instability – termed the "stretch-coil" instability – when moving in the neighborhood of a hyperbolic stagnation point of the flow. When the stagnation point is embedded in an extended cellular flow, it is found that immersed fibers can move as random walkers across time-independent closed-streamline flow. It is also found that the flow is segregated into transport regions around hyperbolic stagnation points and their manifolds, and closed entrapment regions around elliptic points.

PACS numbers: 83.60.Wc,91.60.Ba,87.15.Aa,47.57.eb,47.51.+a,64.75.tg

Simple rheological flows – linear shearing, extensional straining – are often used to probe the mechanical responses of deformable media [1]. For a complex fluid even such simple forcing can induce nontrivial dynamics in the fluid's micro-structure. Shearing a suspension of microscopic fibers beyond a critical shear-rate can induce fiber buckling, leading to the abrupt appearance of normal stress differences [2–5]. Straining a polymer suspension can induce coil-stretch transitions [6], a process recently visualized in strongly mixing elastic flows [7]. The relation between micro-structural dynamics and macroscopic mechanical properties of the fluid is essential to understanding novel dynamics of elastic turbulence and mixing [8].

Buckling instabilities of fibers have also arisen as modulators of transport. Actin filaments (a biological polymer) are observed to be propelled along myosin coated surfaces [9, 10], showing a meandering dynamics with apparent bucklings driving changes in direction. Conceived as a technique for assaying the mechanical properties of such biopolymers, it was proposed that the consequent wandering, perhaps random, motion resulted from spatial inhomogeneity of myosin density on the plate.

Inspired by such observations, we consider the dynamics and transport of elastic fibers in simple time-independent, incompressible cellular flows. We focus on 2D flows, where cellular flows are generically composed of a lattice of hyperbolic fixed points connected by stable/unstable manifolds (converging/diverging flows) and a set of elliptic fixed points (vortices). Without temporal variation, such a closed stream-line cellular flow is a poor mixer as no global mixing between cells can occur in the absence of molecular diffusion. We show that an elastic fiber can be transported across such a flow as a random walker (Fig. 1), with random choices of direction induced by the internal filament dynamics in the neighborhood of hyperbolic fixed points. This is unlike the translational diffusion due to interaction of filaments in dilute or semidilute regimes [11], or the self-diffusion of flexible filaments [12] (and references therein).

Unlaying this transport is a bifurcation, complementary and inverse to the coil-stretch transition. Above a critical strain-rate at a hyperbolic point, a straight filament (the rest state) becomes unstable to buckling and can become folded, or "coiled" for very large strain-rates. This configuration allows the fiber to sample the flow spatially, exiting along one or the other direction of the unstable manifold, and becoming stretched again as it moves to the next fixed point.

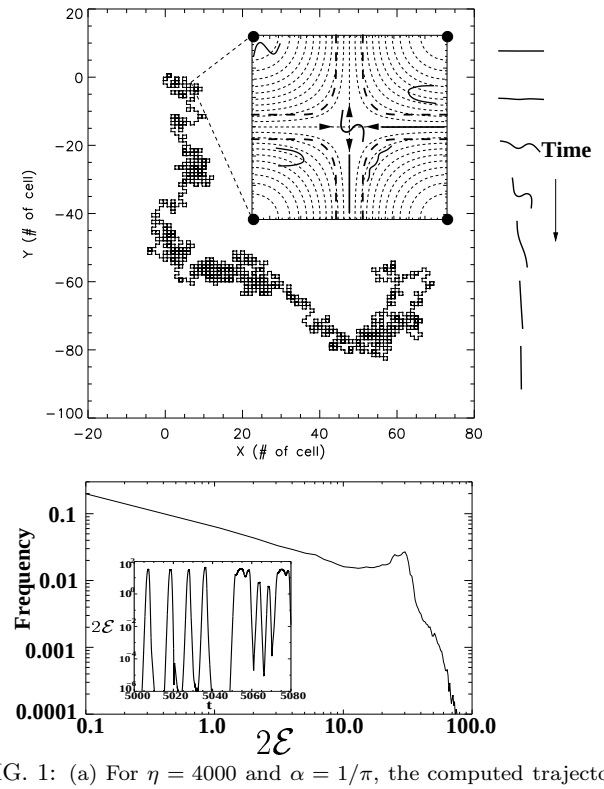

FIG. 1: (a) For $\eta = 4000$ and $\alpha = 1/\pi$, the computed trajectory (for center of mass) of a meandering filament. The box is 100×120 cells. The inset shows the stretch-coil instability as the filament transits through a hyperbolic fixed point (entering/converging from left-right, exiting/diverging to up-down). The thick dashed curves separate regions of transport from entrapment, the dynamics in the latter case shown by the filament shapes within. (b) The histogram of fiber elastic energy $2\mathcal{E}$ for this simulation. The peak at large curvatures corresponds to the persistent stretch-coil transitions at hyperbolic fixed points. The inset shows a sample evolution of $2\mathcal{E}$.

Formulation: Consider a slender, inextensible and elastic filament of radius r, length L, and rigidity E, moving in a Stokesian fluid of viscosity μ with a background velocity field $(W\dot{\gamma})\mathbf{U}(\mathbf{x}/W)$. Here W is the cell size and $\dot{\gamma}$ a strain-rate at a hyperbolic point. The Brownian, inertial, and gravitational forces scale as $k\mathrm{T}/L$, $\rho_f\dot{\gamma}^2L^4$, and $g(\rho_s-\rho_f)r^2L$, respectively for rod-shaped colloidal particles of density ρ_s. In most applications these forces are negligible, and thus are not included in the formulation. We denote the fiber position by its centerline position $\mathbf{X}(s,t)$, where s is arclength, and scale space on the length L, and time on $\dot{\gamma}^{-1}$. According to slender-body theory [13, 14], as used in many other studies (e.g. [2, 15]), the leading order dynamics is governed by a local balance of drag forces with the force of the filament upon the fluid:

$$\eta\mathbf{D}\left(\mathbf{X}_t-\alpha^{-1}\mathbf{U}(\alpha\mathbf{X})\right)=-\left(\mathbf{X}_{ssss}-(\sigma(s)\mathbf{X}_s)_s\right) \quad (1)$$

where $\mathbf{D}=\mathbf{I}-(1/2)\mathbf{X}_s\mathbf{X}_s$ is an anisotropic drag tensor ($\mathbf{D}^{-1}=\mathbf{I}+\mathbf{X}_s\mathbf{X}_s$), $\alpha=L/W$ is the ratio of filament length to cell size, and $\eta\equiv 8\pi\mu\dot{\gamma}L^4/Ec$ is the effective viscosity (with $c=-\log(\epsilon^2 e)$ where $\epsilon=r/L<<1$). Filament forces (per unit length) are described by Euler-Bernoulli elasticity: $\mathbf{f}=\mathbf{X}_{ssss}-(\sigma(s)\mathbf{X}_s)_s$. The line tension σ is determined by the constraint of inextensibility, expressed as $\mathbf{X}_s\cdot\mathbf{X}_{ts}=0$, which yields a 2^{nd}-order boundary value problem that closes with the conditions $\sigma=0$. Zero total force and torque on the filament is satisfied by the "free" boundary conditions $\mathbf{X}_{ss}=\mathbf{X}_{sss}=\mathbf{0}$. Note that with the choice of scaling, α drops out of the dynamics for any linear background flow (e.g. simple strain or linear shear). This system can be posed variationally with Rayleigh dissipation function $\mathcal{D}=(\eta/2)\int ds\ \mathbf{X}_t\mathbf{D}\mathbf{X}_t$, and (elastic) energy, $\mathcal{E}=(1/2)\int ds\ \mathbf{X}_{ss}^2$ (decaying in the absence of forcing).

The Hasimoto transformation is utilized to convert Eq. (1) to an equation for the complex curvature of the filament centerline [16, 17]. The resultant system is numerically integrated (with 2^{nd}-order in space and time) to simulate the filament motion in a given background flow $\mathbf{U}$.

We focus on a simple time-independent, spatially periodic 2D cellular flow, $\mathbf{U}=(\sin x\cos y,-\cos x\sin y,0)$, with hyperbolic fixed points at $(n\pi,m\pi,0)$ for m, n integers (e.g., near (0,0,0), $\frac{1}{\alpha}\mathbf{U}(\alpha\mathbf{x})\approx(-x,y,0)$)). The basic periodic structure contains four cells, or vortices, each of width π, and is similar to a four-roll mill flow [4, 18]. This sets $\alpha=L'/\pi$, with L' the relative filament length.

For $\eta=4000$ and $\alpha=1/\pi$, Fig. 1(a) shows the "meandering" trajectory of an initially straight filament released near a stable manifold ($x=n\pi$ or $y=m\pi$). Its dynamics is roughly this: the filament aligns with the stable manifold as it approaches a hyperbolic fixed point (as in the inset of Fig 1(a)). The viscous stresses produced by the local straining flow begin to compress the filament along its axis, and if sufficiently high, the filament buckles. The now coiled filament samples the local velocity field around the hyperbolic point, and exits along its unstable manifold, the direction chosen with apparent randomness (downward in Fig. 1(a) inset). The consequence of these stretch-coil transitions is filament transport across space as a random walker.

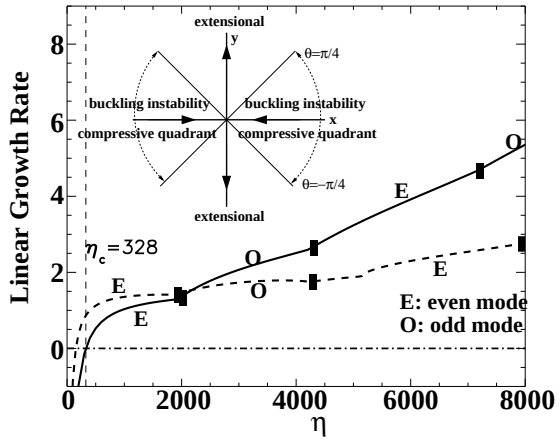

FIG. 2: Linear growth rate versus η for filament with $\theta=0$ at the center of the linearized hyperbolic flow (solid line). The thick dashed line is the growth rate for a filament in planar shear flow. The "E" and "O" labels whether the dominant eigenfunction is even or odd about the filament center point. The inset schematic shows the regions of compressive flow (potentially yielding a buckling instability) and extensional flow around the hyperbolic fixed point for the straining flow $\mathbf{U}=(-x,y,0)$.

Fig. 1(b) shows the (normalized) histogram of elastic energy $\mathcal{E}$ accumulated over long time. Persistent filament buckling along its meandering trajectory corresponds to repetitive stretch-coil transitions, which appear as the high-curvature peak in the histogram. The temporal dynamics of these transitions is illustrated in the inset, showing the time evolution of $2\mathcal{E}$. Its episodic rise and fall, roughly over an order of 10 time units, corresponds to the coiling and stretching of the filament.

The rapid temporal growth in elastic energy results from a buckling instability near the fixed point and can be quantitatively analyzed, as has been done in the shearing case [2, 19]. Firstly, an initially straight filament remains so while moving in any linear background flow. Consider then a nearly straight filament in the straining flow $(x,-y)$ (dropping the third dimension). The linearized dynamics for the perturbation $\mathbf{y}$ from the straight filament is $\eta\mathbf{y}_t=-\mathbf{y}_{ssss}+2\sigma_s\mathbf{y}_s+\sigma\mathbf{y}_{ss}$, where $\sigma(s)=\eta\cos(2\theta)/4(s^2-1/4)$ ($-\eta\sin(2\theta)/8(s^2-1/4)$ for planar shear flow), and $\theta(t)$ is the filament angle with the x axis. If $\theta(t)$ varies slowly, this linear equation can be taken as a homogeneous, constant coefficient PDE linear in $\mathbf{y}$ and is amenable to standard eigenvalue analysis, results from which are shown in Fig. 2.

This analysis reveals that a filament can undergo a compressive buckling instability if moving towards the fixed point in the quadrant $-\pi/4\le\theta\le\pi/4$ around

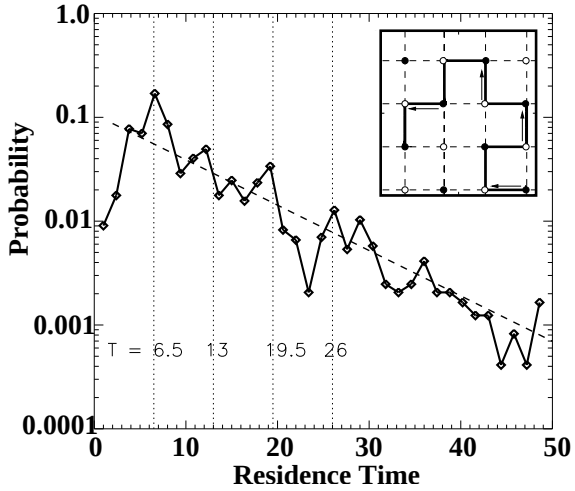

FIG. 3: Frequency of residence time for $\eta = 4000$ and $\alpha = 1/\pi$. The dashed line is a prediction from Eq. (2). The inset schematic shows an idealized filament trajectory across the network of hyperbolic points. The vertical dashed lines correspond to the frequency peaks.

the stable manifold, as illustrated in the inset of Fig. 2. This instability appears at finite η (i.e., for a sufficiently flexible filament, or sufficiently high strain-rate, etc.); for $\alpha = 1/\pi$, as in the simulation of Fig. 1, the instability appears for $\eta > \eta_c$, with $\eta_c \approx 328$. We refer to the instability boundary in (η, α) as the stretch-coil transition boundary, and it is plotted (bottom dashed line) in Fig. 5.

It is this instability that drives the meandering dynamics observed in Fig. 1. For this simulation Fig. 3 shows the residence time frequency, where residence time is the time a fiber moves within a particular cell. This frequency plot is multiply peaked and shows an overall exponential decay. A very simple model of this dynamics is as a walker moving on the lattice of hyperbolic points, as illustrated in the Fig. 3 inset. If we assume that the choice of particle exit direction (up or down at open circles; left or right at closed circles) is made with equal probability of 1/2, and is independent of the previous choice, then neglecting recurrences the discrete probability distribution for residence time T is given by

$$P(T) = (\ln 2/\Delta T)(1/2)^{T/\Delta T} \qquad (2)$$

where $T = N\Delta T$ with ΔT the transit time between lattice points. With no a priori estimate available, the value of ΔT in the exponential distribution plotted in Fig. 3 is taken as the location of the first and highest peak of the residence time frequency. The discrete probability captures the successive peaks in the frequency plot, each corresponding to successive direction choices that keep the filament within a single cell.

Given the average transit time ΔT, the effective filament diffusivity is given by $D \equiv \alpha^{-2}/4\Delta T$. Taking $\Delta T \sim 6.5$ and $\alpha = 1/\pi$ gives $D \sim 0.38$. The effective filament diffusivity can also be estimated from the fiber dispersion $d^2(t)$ [11], which for a Brownian walker satisfies $d^2 \sim 4Dt$ for large t. Fig. 4 shows d^2 estimated by an ensemble average of eighty simulations for different initial filament placements (same location for the filament center but different filament angle with the x-axis), for $\alpha = \pi^{-1}$ and for various η. Each plot shows a roughly linear increase in time, consistent with random walk statistics. The plot for $\eta = 4000$ (curve 2) is overlaid by a dashed line of slope $4D$ with $D = 0.38$, showing consistency with the estimate of D found using the residence time frequency distribution. The figure also suggests that the effective diffusion remains almost identical for $4000 \leq \eta \leq 7000$ (curves 2, 3, and 4), but decreases for $\eta = 527.4$ (curve 1), which is slightly above η_c, the critical value for instability. For increasing η, the implied diffusion is non-monotonic, increasing towards $\eta = 8000$ (curve 5), then monotonically decreasing at yet higher values (curves 6 and 7). For $\eta = 15708$ the filament is curved and trapped inside the cell, as shown schematically in Fig. 5, and no diffusive transport is found.

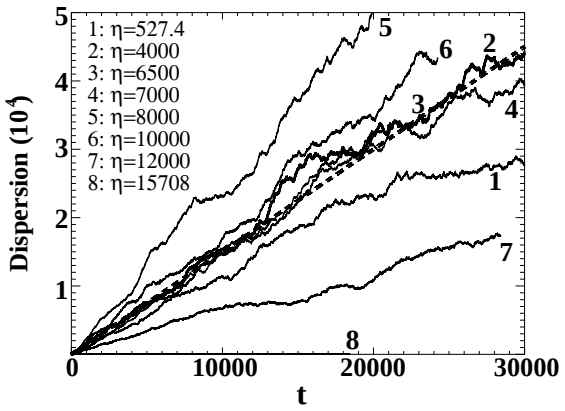

FIG. 4: Filament dispersion versus time for $\alpha = 1/\pi$ and various η, each estimated by an ensemble average of eighty simulations. The dashed line is the dispersion estimate for a random walker, $d^2(t) = 4Dt$, using the estimated diffusion $D = 0.38$ for $\eta = 4000$ (*cf.* curve 2).

Fig. 5 depicts the transitions in filament dynamics in the $\eta - \alpha$ plane. For all values of α, no buckling instability occurs for η below η_c, which almost coincides with the lower boundary of transport (solid line) from simulations. Below the lower boundary a filament either settles to a fixed point or stays trapped within a cell. For $\eta_c < \eta <\sim 1.5 \times 10^4$, diffusive filament transport (meandering) is found if the filament is released not too far from the manifolds. The inset graph shows the estimated probability of a filament being trapped in the cell as a function of its initial distance to a manifold. We define the size of the transport region by the distance that corresponds to 50% for the trapping probability. For $\alpha = 1/\pi$ this distance is ~ 0.2 (see the dashed curves in the inset of Fig. 1a), and seems insensitive to η. For yet larger η the region of transport collapses, and the filament is trapped in the interior as illustrated in the inset.

Finally, to seek some comparison with experimental observation, Fig. 6 shows the computed distributions for

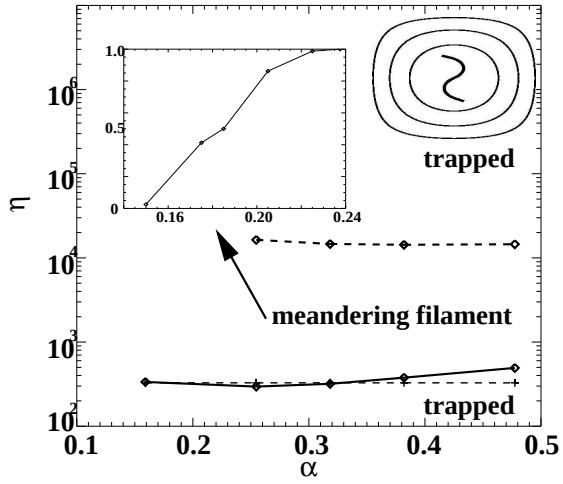

FIG. 5: Phase diagram of filament dynamics in cellular flow. For a given filament length (scaled to the cell size), there exists a range of effective viscosity for meandering elastic filament. The dashed line is the threshold to stretch-coil instability. Inset on the lower left shows the probability for the meandering filament to be trapped in the cell as a function of initial distance to the manifold for $\alpha = 1/\pi$. Inset on the upper right corner is for filament length $\alpha = 1.5/\pi$ and $\eta = 80000$. Animations of filament dynamics for different values of η and $\alpha = 1/\pi$ can be found at [20]

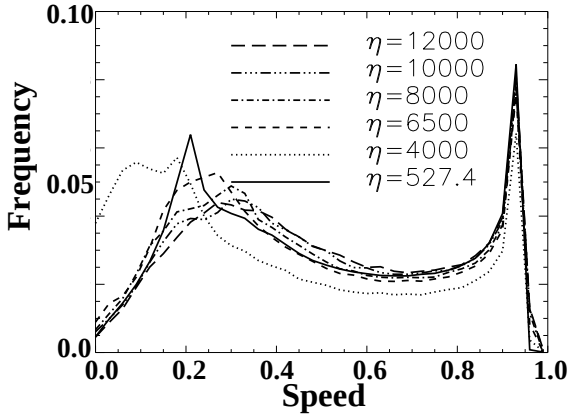

FIG. 6: The probability of filament center-of-mass speed at different values of effective viscosity.

the speed of meandering filaments, again for $\alpha = 1/\pi$ and for various η. These distributions are essentially bimodal, as was observed in the actin transport experiments of Bourdieu *et al.* [9, 10] at higher myosin densities. The bimodality reflects the basic dynamics underlying filament transport. The sharp peak for all distributions near speed of unity is that associated with transport between successive hyperbolic point. The secondary peak at lower velocities reflects the "loitering" of filaments near hyperbolic points as the buckling instability develops, and which seem to be influenced by its geometric details. For $\eta_c < \eta < 2000$ the buckling instability is manifested by an even mode (Fig. 2), with the secondary peak moving to the right as η increases in this range. For $\eta > 2000$, competition between even and odd modes can lead to a more complex distribution ($\eta = 4000$ for example), and the more prominent the odd mode the more the secondary peak moves towards lower speeds. As the even mode takes over for η above 4250, the secondary peak shifts towards the right.

We have found similar dynamics in three-dimensional cellular flows, though the details can depend on the particular choice made. We are currently studying the 3D case more deeply, as well as the nature of extra-stress contributions made by action of the stretch-coil transition. On this, an interesting question is whether dynamically complex flows can be generated by suspensions of semi-flexible polymers [21], as has been demonstrated for dilute polymer-coil suspensions, and if so, what is the role of microstructural instabilities as studied here.

Acknowledgments. We acknowledge support from the NSF though DMS-0412203 (MS) and DMS-0420590 (NJIT), from the DOE through DE-FG02-88ER25053 (MS), and from NJIT through a SBR grant (YNY).

[1] R. Larson, *The Structure and Rheology of Complex Fluids* (Oxford University Press, 1998).
[2] L. E. Becker and M. Shelley, Phys. Rev. Lett. **87**, 198301 (2001).
[3] S. Lin-Gibson, J. A. Pathak, E. A. Grulke, H. Wang, and E. K. Hobbie, Phys. Rev. Lett. **92**, 048302 (2004).
[4] X. Li and K. Sarkar, Phys. Rev. Lett. **95**, 256001 (2005).
[5] D. Fry, B. Langhorst, H. Kim, E. Grulke, H. Wang, and E. K. Hobbie, Phys. Rev. Lett. **95**, 038304 (2005).
[6] P. G. D. Gennes, J. Chem. Phys. **60**, 5030 (1974).
[7] S. Geraschenko, C. Chevallard, and V. Steinberg, Europhys. Lett. **71**, 221 (2005).
[8] A. Groisman and V. Steinberg, Nature **405**, 53 (2000), **410**, 905 (2001); New Journal of Phys. **4**, 74437 (2004).
[9] L. Bourdieu, T. Duke, M. B. Elowitz, D. Winkelmann, S. Leibler, and A. Libchaber, Phys. Rev. Lett. **75**, 176 (1995).
[10] L. Bourdieu, M. O. Magnasco, D. Winkelmann, and A. Libchaber, Phys. Rev. E **52**, 6573 (1995).
[11] M. Rahnama, D. L. Koch, Y. Iso, and C. Cohen, Phys. Fluids **5**, 849 (1993).
[12] Z. Bu, P. S. Russo, D. L. Tipton, and I. I. Negulescu, Macromolecules **27**, 6871 (1994).
[13] R. E. Johnson, J. Fluid Mech. **99**, 411 (1980).
[14] I. Klapper, J. Comp. Phys. **125**, 325 (1996).
[15] R. E. Goldstein, T. R. Powers, and C. H. Wiggins, Phys. Rev. Lett. **80**, 5232 (1998).
[16] K. Nakayama, H. Segur, and M. Wadati, Phys. Rev. Lett. **69**, 2603 (1992).
[17] R. E. Goldstein and S. A. Langer, Phys. Rev. Lett. **75**, 1094 (1995).
[18] P. E. Arratia, C. C. Thomas, J. Diorio, and J. P. Gollub, Phys. Rev. Lett. **96**, 144502 (2006).
[19] T. Munk, O. Hallatschek, C. H. Wiggins, and E. Frey, Physical Review E **74**, 041911 (2006).
[20] `http://harp.njit.edu/~yyoung/stretch-coil.html`.
[21] A.-K. Tornberg and M. Shelley, J. Comp. Phys. **196**, 8 (2004).